Thin films composed of Ag nanoclusters dispersed in TiO_2: influence of composition and thermal annealing on the microstructure and physical responses

J. Borges[1*], M.S. Rodrigues[2,3], C. Lopes[2], D. Costa[2], F.M Couto[4], T. Kubart[5], B. Martins[3], N. Duarte[3], J. P. Dias[3], A. Cavaleiro[6], T. Polcar[1,7], F. Macedo[2], F. Vaz[2,6]

[1]Department of Control Engineering, Faculty of Electrical Engineering, Czech Technical University in Prague, Technická 2, Prague 6, Czech Republic

[2]Centro de Física, Universidade do Minho, Campus de Gualtar, 4710 - 057 Braga, Portugal

[3]Instituto Pedro Nunes, Laboratório de Ensaios, Desgaste e Materiais, Rua Pedro Nunes, 3030-199 Coimbra, Portugal

[4]Physics Sciences Laboratory, Norte Fluminense State University, 28013-602, Campos –RJ, Brazil

[5]Solid-State Electronics, Department of Engineering Sciences, Uppsala University, P.O. Box 534, Uppsala SE-751 21, Sweden

[6]SEG-CEMUC, Mechanical Engineering Department, University of Coimbra, 3030-788 Coimbra, Portugal

[7]National Centre for Advanced Tribology at Southampton (nCATS), University of Southampton, Highfield, SO17 1BJ Southampton, UK

Corresponding author: *joelborges@fisica.uminho.pt

Abstract

Noble metal powders containing gold and silver have been used for many centuries, providing different colours in the windows of the medieval cathedrals and in ancient Roman glasses. Nowadays, the interest in nanocomposite materials containing noble nanoparticles embedded in dielectric matrices is related with their potential use for a wide range of advanced technological applications. They have been proposed for environmental and biological sensing, tailoring colour of functional coatings, or for surface enhanced Raman spectroscopy. Most of these applications rely on the so-called localized surface plasmon resonance absorption, which is governed by the type of the noble metal nanoparticles, their distribution, size and shape and as well as of the dielectric characteristics of the host matrix. The aim of this work is to study the influence of the composition and thermal annealing on the morphological and structural changes of thin films composed of Ag metal clusters embedded in a dielectric TiO_2 matrix. Since changes in size, shape and distribution of the clusters are fundamental parameters for tailoring the properties of plasmonic materials, a set of films with different Ag concentrations was prepared. The optical properties and the thermal behaviour of the films were correlated with the structural and morphological changes promoted by annealing. The films were deposited by DC magnetron sputtering and in order to promote the clustering of the Ag nanoparticles the as-deposited samples were subjected to an in-air annealing protocol. It was demonstrated that the clustering of metallic Ag affects the optical response spectrum and the thermal behaviour of the films.

Keywords: Thin films; Ag clusters dispersed in TiO_2; localized surface plasmon resonance; thermal behaviour.

1. Introduction

Materials tailored at the nanoscale, e.g. in the form of nanoparticles, have unique physical and chemical properties compared to their bulk form [1]. Among them, silver (Ag) and gold (Au) are the two most studied plasmonic materials since when they are embedded in a dielectric matrix they manifest localized surface plasmon resonances (LSPR) in the visible range [2] [3] [4]. The LSPR effect occurs when the metallic nanoparticles are well-separated and have dimensions significantly smaller than the wavelength of the incident electromagnetic field [3]. It is responsible for a broad and intense absorption of light in the vicinity of the resonance frequency and the enhancement of the local electromagnetic field [1]. The LSP resonance frequency, bandwidth and peak height depend markedly on the nanoparticles composition, their shape, size and size distribution and also on the host dielectric matrix [5]. The well-known dependence of LSPR on the refractive index of the surrounding medium is also particularly important for the detection of chemical and biological species [6] [7]. In this particular point, the use of high sensitive and low cost plasmon-based optical sensing platforms can be useful in a wide range of fields such as food quality and safety, medical diagnostics and environment monitoring [7] and in Surface-Enhanced Raman Scattering (SERS) [8] [9]. The latter example is a well-established analytical technique used for the detection and recognition of molecular species even if they are in very low concentration; however it depends on the development of high-quality SERS active substrates being an area of great interest for the scientific community [8] [9] [10] [11].

Due to its chemical inertness and biocompatibility, Au is the preferred noble metal for biological applications [2]. However, Ag is preferable in some cases for example in SERS since it can produce higher enhancement factors [8] [9].

In recent works it was studied the influence of gold concentration, dispersed in a TiO_2 matrix, and annealing temperature on the microstructural features and optical response of Au:TiO_2 thin films [12] [13] [14] [15]. The overall set of results showed that the growth of Au nanoparticles/clusters with different sizes and size distributions is highly dependent of the annealing temperature [14] and, on the other hand, the intermediate Au contents, i.e. between 5 at.% and 15at.%, can produce a spectrally broad LSPR bands [16] [17]. At the same time, it was also observed the crystallization of the TiO_2 host matrix in anatase (from 400 ºC) and rutile (from 700 ºC).

In this work, several thin films with a wide variation of silver noble metal (Ag) concentrations were prepared by magnetron sputtering deposition using a Ti target with small

pellets of Ag placed on the preferred erosion zone. In order to study the influence of Ag concentration and annealing temperature on the microstructure of the films and how those features are correlated with the optical and thermal properties of Ag:TiO_2 films, the samples were subjected to a thermal treatment in air atmosphere.

2. Experimental details

The thin films, composed of silver (Ag) dispersed in a TiO_2 matrix, were deposited by reactive DC magnetron sputtering in a home-made deposition system. More details about the system can be found elsewhere [18].

For the deposition of the thin films it was used a titanium target (200×100×6 mm^3, 99.8% purity) containing various amounts of Ag pieces, or "pellets" (thickness: 1 mm, disk area: 16 mm^2). The pellets were placed on the preferred erosion zone of the Ti target ("erosion track"). In each deposition, the number of Ag pellets was increased (from 1 to 6) in order to enhance the flux of Ag atoms towards the substrate. The purpose of this methodology was to obtain thin films with different Ag concentrations. The DC power supply was set to operate in the current regulating mode, using a constant current density of 100 $A.m^{-2}$ on the Ti-Ag target. The films were prepared using a gas atmosphere composed of Ar (partial pressure of 4.0×10^{-1} Pa) and O_2 (partial pressure of 5.6×10^{-2} Pa). The working pressure (about 4.5×10^{-1} Pa) was constant during the deposition of the film. The oxygen partial pressure was chosen according to the hysteresis experiment, which is described in [14]. Moreover, the conditions described above are similar to those used to produce the Au:TiO_2 system [14], where the Au pellets are here "replaced" by Ag.

The films were deposited onto silicon with (100) orientation, for characterization purposes (composition, structure and morphology); glass (ISO 8037) and fused silica (SiO_2), for the optical and thermal characterizations. The substrates were placed in a grounded (GND) rotating holder (9 r.p.m.), heated at 100 ºC using a resistor. Prior to depositions, the substrates were subjected to an in-situ etching process by applying to them a pulsed DC current of 0.5 A (T_{on}= 1536 ns and f = 200 kHz) during 1200 s, in a pure argon atmosphere (partial pressure of 4.0×10^{-1} Pa).

After the deposition of the films, an in-air annealing process was carried out in order to promote the Ag clustering, as consequence of Ag diffusion throughout the host matrix. In this way it is possible to tailor the structural and morphological features of the plasmonic nanostructures. The annealing temperatures used were between 200 and up to 800 ºC, with a

heating ramp of 5 ºC/min. and an isothermal period of 1 h. The samples were let to cool down freely and then removed from the furnace, after they reached the room temperature.

The chemical composition of the films was analysed by Energy-dispersive X-ray Spectroscopy (EDS), using a JEOL JSM-5310/Oxford X-Max.

The structural analysis of the coatings was carried out using Grazing Incidence X-Ray Diffraction (GIXRD), with a Philips X-Pert diffractometer (Co-Kα radiation), operating at an angle θ = 2º. The scans were done between 15º and 80º, with a scan step of 0.025º and an acquisition time of 1 s. By using the Winfit software, the XRD patterns were deconvoluted, assuming to be Pearson-VII functions in order to estimate the grain size of the clusters from the integral breadth method.

The morphological features in cross section view were probed by scanning electron microscopy (SEM), using a Zeiss Merlin instrument, equipped with a field emission gun and charge compensator. Both in-lens secondary electron and energy selective backscattered electron detectors were employed. The growth rate was calculated by the ratio between the average thickness (estimated by cross-section SEM analysis) and deposition time (90 min.).

The films transmission coefficients (300-900 nm) were measured in glass, for annealing temperatures up to 500 ºC, and in fused SiO_2 substrates, for annealing temperatures above 500 ºC. The measurements were performed in a Shimadzu UV-3101 PC UV–Vis–NIR.

For thermal properties measurements a non-stationary photothermal technique, namely modulated infrared photothermal radiometry (MIRR) [19] was used. Basically, the sample is heated with an intensity modulated laser beam and the infrared response at the same frequency is recorded. The experimental setup uses a DPSS 532nm laser for excitation and an acousto-optic modulator to modulate the incident light from nearly DC up to 100kHz. A set of two BaF_2 lenses are used for collecting and focusing the infrared response from the sample into an IR HgCdTe detector. The resulting electric signal is then pre-amplified and fed into a lock-in SR830. All the data acquisition process is controlled by software. Extensive information and details on the technique can be found elsewhere [20] [21]. Since the penetration depth of the generated “thermal waves” depend inversely on the modulation frequency, this technique is particularly useful to study thin films and coatings. From the behaviour of the amplitude and phase lag of recorded signals, the thermal diffusion time and the thermal effusivity ratio can be estimated using the two-layer model proposed by Fotsing et al. [22]. Knowing the thermal diffusion time and the thickness, measured by SEM, the thermal diffusivity can be immediately calculated.

3. Results and discussion

3.1 Deposition characteristics, structure and morphology of the films

3.1.1 Deposition characteristics of the Ag:TiO_2 system

It is well known that the processing conditions (discharge conditions, plasma composition, deposition characteristics, etc.) should be carefully selected since they are of paramount significance for the microstructural (structure, morphology, phase composition) evolution of the films during its growth and hence for the final overall physical responses [23].

In order to study some of those deposition-related features, the evolution of the target (cathode) potential during the growth of the film, as well as the deposition (growth) rate of the films were firstly analysed. The values of those parameters are plotted in Fig. 1 as a function of the Ag pellets area, including a film without Ag. The number of pellets varied between 1 and 6, corresponding to a silver area variation from 16 to 96 mm^2. For the target without Ag pellets the cathode potential was about 486 V. This value results from the addition of oxygen to the chamber with a partial pressure that ensures the "poisoning" of the target surface with a superficial oxide layer (compound regime of the target), as already discussed elsewhere [14]. The cathode potential of the oxidised target is therefore much higher than the value found during the sputtering of Ti only with Ar (about 320 V), which is a typical behaviour of the reactive sputtering process [24].

Taking into account the uncertainty of the measurement of the target potential (about 4 V), it seems that the cathode voltage is not significantly affected by the presence of Ag pellets in the Ti target and thus one can report that the target potential remains approximately constant up to 6 Ag pellets (area of 96 mm^2). On the other hand, the growth rate evolution of the as-deposited films seems to follow two different trends; approximately constant up to 3 Ag pellets (~4 $nm.min^{-1}$), and sharply increasing as area of Ag pellets was progressively enlarged, changing from 4 to about 10 $nm.min^{-1}$, Fig. 1.

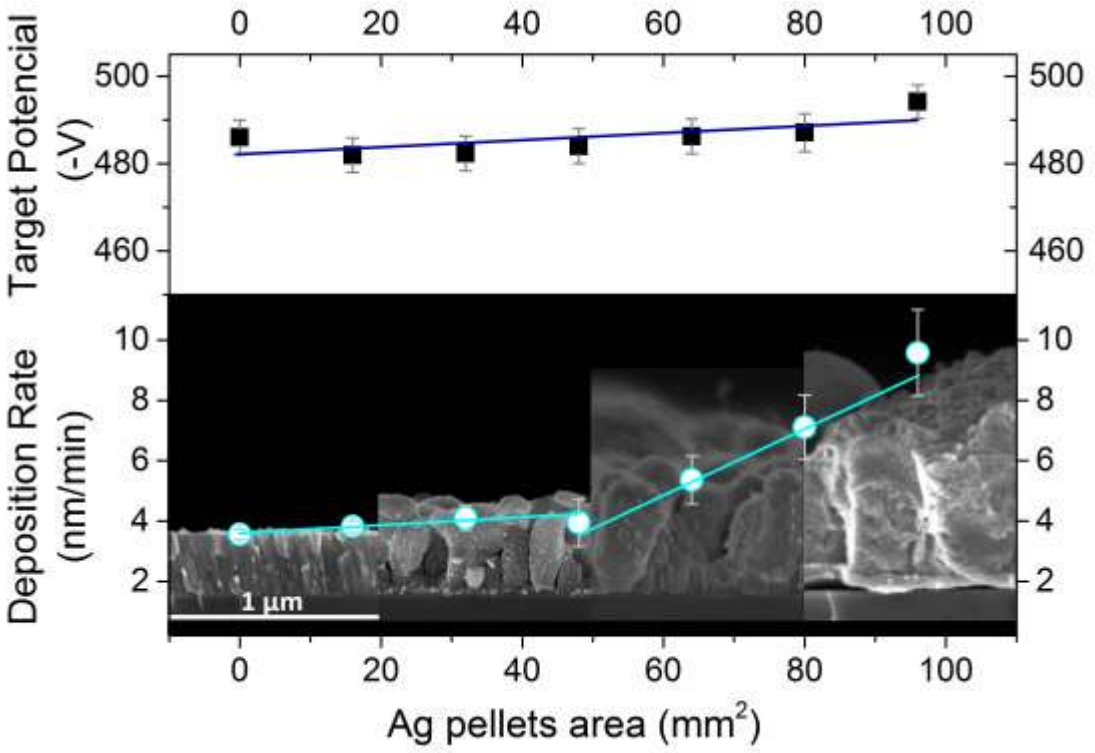

Figure 1 – Target potential and deposition (growth) rate of the films as a function of the Ag pellet area. The cathode voltage was monitored during the entire deposition and each data point corresponds to the equilibrium target potential, reached after the first 300s of deposition. Selected cross-sectional SEM images are also embedded in the figure (all with the same scale), corresponding to as-deposited samples with Ag pellets area of 16, 64, 80 and 96 mm^2 (from left to right).

In order to explain the behaviour of the cathode potential induced by modifications of the surface of the target, the well-known Thornton equation is often used [25]. Since the discharge sustaining mechanism in sputtering is based on the emission of secondary electrons from the target due to ion bombardment, the main factor affecting the minimal voltage to sustain the discharge (V_{min}) is the effective secondary electron emission yield (γ_{eff}), where $V_{min} \alpha 1/\gamma_{eff}$ [25]. The effective yield (γ_{eff}) is proportional to the ion induced secondary electron emission (γ_{ISEE}) coefficient and according to studies developed by D. Depla *et al.* [25], the γ_{ISEE} coefficients of Ti and Ag are rather close, about 0.114 and 0.110, respectively [26]. However, the Ti target is poisoned with oxide and the corresponding γ_{ISEE} coefficient is lower; about 0.078 according to D. Depla *et al.* [25]. Therefore, in principle, the γ_{ISEE} coefficient of the composite target (with Ag pellets) should increase with the incorporation of silver and the target potential hence decrease; assuming that the γ_{ISEE} coefficient of Ag

remains approximately constant, since there is no evidence of the silver oxidation. Anyway, the results displayed in Fig. 1 show that the Ag placed at the target surface was not enough to significantly disturb the discharge characteristics, similarly to what was reported for the Au:TiO_2 system [14]. This is a consequence of the low fraction of silver used to produce the films, always less than 1 % of the total area of the Ti target.

Although the area of Ag exposed to the plasma was typically low, the growth rate of the films increased with the number of pellets. To explain this behaviour there are two effects to be considered. On the one hand, the amount of sputtered material is significantly enhanced by the presence of silver since its sputtering yield is much higher than TiO_2 [27] [28]. On the other hand, and since the deposition rate calculation was performed based on the thickness of the film and not on the "real" amount of material deposited, one has to consider the possibility of density changes caused by the different microstructures developed during film growth. This feature can be understood by the analysis of the SEM micrographs embedded in Fig. 1. As it can be observed, the type of growth of the films abruptly changes from the typical columnar growth, for very low contents of Ag, towards more porous and granular microstructures as the Ag content increases.

3.1.2 Composition of the films

As expected from the previous analysis of the growth rate evolution, the atomic concentration (at. %) of Ag in the films is correlated with the number of Ag pellets placed in the Ti target. These results are displayed in Fig. 2, where it is plotted the molar fraction of silver [χ_{Ag}= n(Ag)/n(Ag+TiO_2)] as a function of the Ag pellets area. It was observed an almost linear increase of Ag concentration in the films. This could mean that the much higher sputtering yield of silver is controlling the composition evolution process. The molar fraction of Ag increases steadily from χ_{Ag}=0.16 (C_{Ag}= 6 at.%) to χ_{Ag}=0.40 (C_{Ag}= 18 at.%), with the increase of number of Ag pellets from 1 (16 mm^2) to 6 (96 mm^2). The elemental concentration analysis also revealed that the C_O/C_{Ti} atomic ratio was always very close to 2 in all samples, thus confirming the formation of a close-stoichiometric TiO_2 matrix.

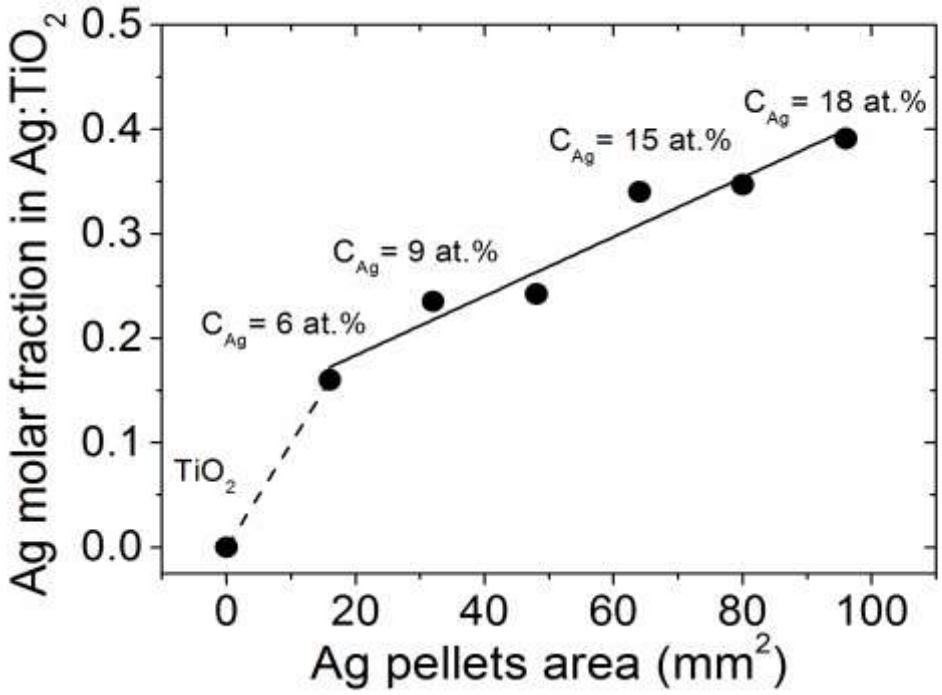

Figure 2 – Ag molar fraction (χ_{Ag}), and the corresponding concentration (at. %), in the TiO_2 matrix as a function of the Ag pellets area.

3.1.3 Influence of heat-treatment on the structure of the films

It is well-known that the optical response of a plasmonic nanocomposite film, especially in what concerns the formation of a LSPR absorption band, depends on the capability of stabilizing noble nanoparticles, with specific sizes, distributions and shapes, inside a dielectric matrix. It was demonstrated in recent works that annealing treatments can control, by diffusion processes, those features related to the nanoparticles and at the same time the matrix crystallinity [13] [17] [29] [30].

In order to promote some (micro)structural changes that are required to tailor the LSPR effect and hence the optical response of the films, the as-deposited samples were heat-treated in air from 200 ºC to 800 ºC. The structural evolution of the films was studied by grazing incidence XRD as a function of the annealing temperature for the different Ag contents. The diffractograms of pure TiO_2 and of the Ag:TiO_2 films are displayed in Figs 3(a-e).

For TiO_2 samples, Fig. 3(a), the structure is amorphous up to 200 ºC and afterwards the peaks related to anatase (*a*-TiO_2) [ICDD card No. 84-1286] start to appear from the temperature of 300 ºC and up to 800 ºC. The two most intense peaks of *a*-TiO_2 were detected at the 2θ positions of 29.5º (101) and 44.3º (004). It was also possible to identify two other

diffraction peaks related to anatase at the positions 56.5º (200) and 63.6º (105).. Furthermore, a peak related to rutile (*r*-TiO_2) was only observed when the annealing temperature was increased up to 800 ºC [ICDD card No. 88-1172], positioned at 32.1º (110), Fig. 3(a).

The XRD analysis of the films containing Ag, Figs. 3(b-e), revealed no diffraction peaks for the as-deposited samples with low molar fractions of Ag, χ_{Ag} of 0.16 (6 at.%) and 0.24 (9 at.%); and a very broad peak, located in the 2θ angle range 36-42º, for the samples with higher Ag concentration (χ_{Ag}= 0.35 and 0.40), typical of quasi-amorphous structures. These results are also consistent with the formation of an amorphous TiO_2 matrix as shown in Fig. 3(a).

The XRD patterns of the Ag:TiO_2 films show a progressive crystallization of the films as the annealing temperature was increased. As expected, Ag crystallizes in its typical face centred cubic (fcc) structure [ICDD card No. 87-0717], as can be observed by the presence of XRD peaks located at 2θ angular positions of 44.5°, 51.9° and 76.5°, corresponding to (111) , (200) and (220) orientations, respectively.

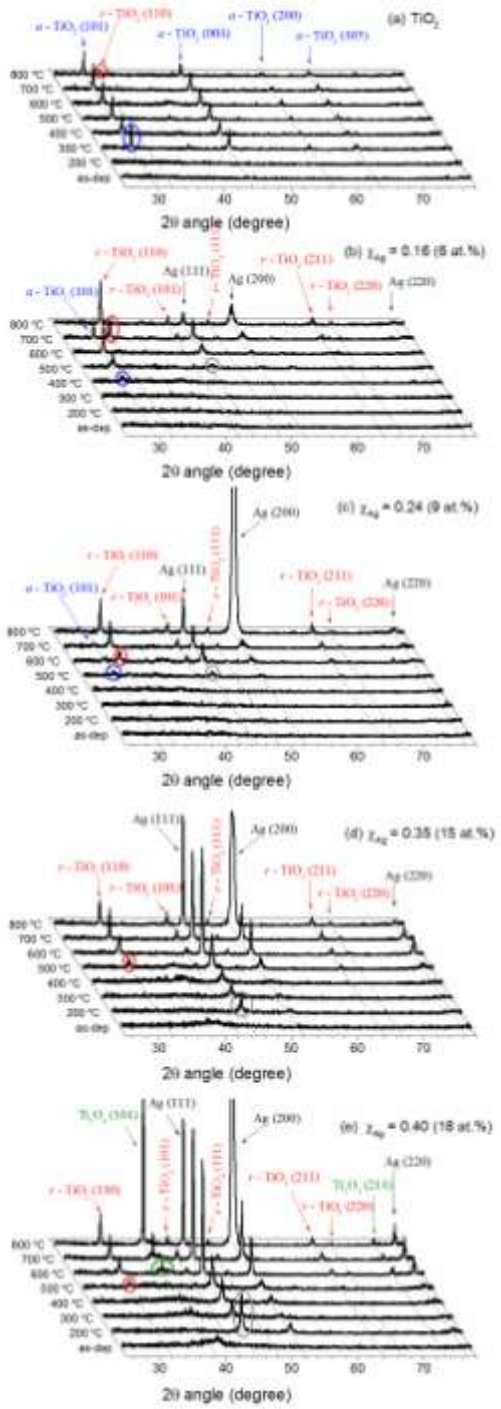

Figure 3. X-ray diffractograms of the different sets of prepared samples as a function of the annealing temperature.

As stated before, the annealing treatment was done primarily to promote the silver diffusion with the aim of growing Ag clusters and/or nanoparticles throughout the host TiO_2 matrix. However, if the Ag molar fraction is low (χ_{Ag} = 0.16) it seems difficult to obtain crystalline domains at low annealing temperatures; since the Ag diffraction peaks are only

visible when the annealing temperature attains 500 ºC. These peaks are broad and can be indexed to the (111) and (200) orientations. As the annealing temperature was increased, they have become sharper and enhanced (between 600 and 800 ºC). Furthermore, at 800 ºC the peak (200) becomes more intense than (111).

For the sample with a molar fraction of $\chi_{Ag} = 0.24$ (9 at.%), the Ag crystallization occurs again from the temperature of 500 ºC, Fig. 3(c), similarly to the sample with $\chi_{Ag} = 0.16$ (6 at.%). As the temperature increases from 600 to 800 ºC the Ag peaks, namely with (111) and (200) orientations, are gradually becoming sharper. As observed in the previous sample ($\chi_{Ag} = 0.16$), the film with $\chi_{Ag} = 0.24$ also revealed a preferred orientation of the Ag crystals up to 700 ºC, Ag (111), changing for Ag (200) at 800 ºC. Furthermore, the sharper peaks observed between 600 and 800 ºC suggest the formation of large crystalline domains of Ag, as it will be seen below in Fig. 5.

When the Ag content further increases, such as the case of the sample with a molar fraction of $\chi_{Ag} = 0.35$ (15 at.%) the formation of small crystalline domains of Ag takes place already at 200 ºC. In the range up to 500 ºC the Ag peaks, (111) and (200), are broad, but still progressively enhanced. Moreover, for higher annealing temperatures (600-800 ºC), the Ag peaks become very sharp and intense.

Finally, the XRD analysis performed to the sample with the higher Ag amount, $\chi_{Ag} = 0.40$ (18 at.%), shows that the behaviour of Ag is similar to the previous sample, despite the peaks seems to be more intense. Once again there is a clear difference between the samples annealed up to 500 ºC, which revealed peaks not very sharp, and the ones between 600 and 800 ºC, where the Ag peaks sharpen and are much more intense, which suggests the formation of large crystalline domains of Ag.

Other important features that can be reported from the XRD analysis are related with the evolution of the matrix crystallization of the films containing Ag when they are subjected to the annealing process. The sample with the lowest Ag concentration, $\chi_{Ag} = 0.16$ (6 at.%), started to crystallize at an annealing temperature of 400 ºC, as the appearance of the diffraction peak of *a*-TiO_2 (101) demonstrates (Fig.3(b)). The intensity of this peak is enhanced up to 600 ºC and then lowers again at 700 ºC, vanishing at 800 ºC. For lower temperatures (T < 400 ºC), the films exhibited very broad XRD patterns, consistent with amorphous-type structures. The rutile phase of TiO_2, *r*-TiO_2, starts to be detected at 700 ºC, increasing in intensity up to 800 ºC. Important to notice is the sample annealed at 700 ºC, where both anatase and rutile structures coexist. It is also worth mentioning that the peaks

related to *a*-TiO_2 are very faint for the samples with low Ag content (χ_{Ag} = 0.16, 0.24) and that the presence of Ag in the TiO_2 matrix increases the crystallization temperature of the anatase phase. The formation of *a*-TiO_2 crystallites was systematically delayed from 300 ºC (pure TiO_2) to 400 ºC (χ_{Ag} = 0.16) or even to 500 ºC (χ_{Ag} = 0.24), where the grain growth is almost inhibited. Moreover, for the highest Ag concentrations (χ_{Ag} > 0.24) the growth of *a*-TiO_2 grains is totally inhibited up to 800 ºC. At the same time, and in opposite tendency, the annealing temperature at which the crystallization of rutile (*r*-TiO_2) starts to occur is progressively reduced as the Ag concentration increases. According to the XRD results displayed in Fig. 3, the heat-treatment promotes *r*-TiO_2 crystallization at only 800 ºC for pure TiO_2. However, this transition temperature decreases to 700 ºC for the film with χ_{Ag} = 0.16 (6 at.%), lowers to 600 ºC for the film with χ_{Ag} = 0.24 (9 at.%) and drops even more to 500 ºC for higher Ag molar fractions, such as the cases of both χ_{Ag} = 0.35 (15 at.%) and 0.40 (18 at.%).

The delay in the crystallization of anatase in Ag:TiO_2 films has been already reported in other works [27] [31] and it is attributed to the increase of the activation barrier for crystallization by the Ag atoms, which are assumed to be fine distributed throughout the amorphous matrix [30]. Therefore, the nucleation of silver to form clusters during thermal annealing slows down the re-arrangement of Ti-O bonds, preventing its crystallization. Another possible effect that cannot be disregarded is the possibility of silver being oxidised as a result of the reactive atmosphere (Ar+O_2) used in sputtering process. In this case, part of the thermal energy transferred during annealing is used to dissociate Ag-O bonds that might exist on the deposited film. Nevertheless, the latter effect might be residual taking into account the XPS analysis performed to a representative sample, before (as-deposited) and after heat-treatment (500 ºC). In fact, the spectra shown in Fig. 4 did not show important shifts in Ag-3d binding energies, remaining practically unchanged after annealing at air atmosphere. This might suggest that Ag is predominately in the metallic state, although some oxidation cannot be disregarded.

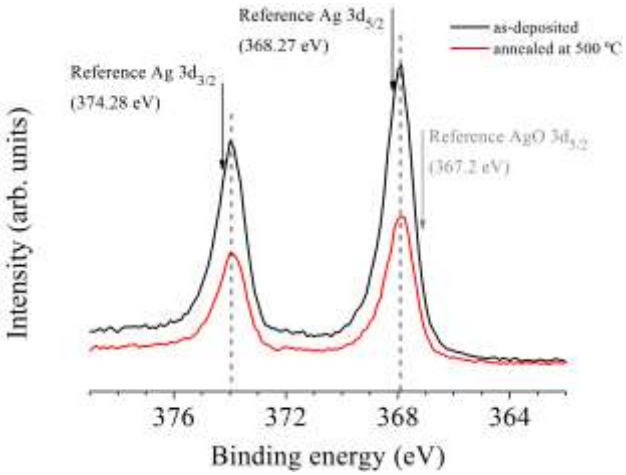

Figure 4. XPS spectra showing the Ag-3d peaks of a representative sample of Ag:TiO_2, as-deposited and annealed at 500 ºC (χ_{Ag} = 0.35). The shown spectra were done with ion cleaning and did not change with depth.

Therefore, silver can be considered as a rutile promoter from amorphous and/or anatase structures since it lowers its transition temperature. As pointed out by A.A. Mosquera *et al.* [31], silver enables a phase control over the film which can be useful for devices based on anatase or rutile TiO_2.

3.1.4 Evolution of the average grain size of the Ag clusters

Figure 5 shows the results of the average grain size of the Ag clusters obtained by XRD peak fitting. The grain size was calculated based on the integral breadth method and using Pearson VII distributions to fit the XRD peaks. For the average grain size calculation it was taken into account, when possible, the peaks indexed to three different orientations present: Ag (111), (200) and (220).

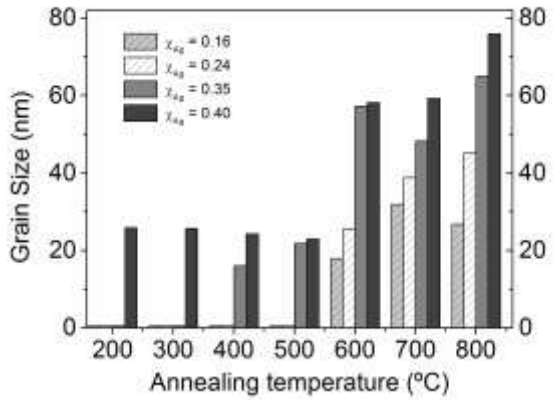

Figure 5 – Comparison of the average grain size of the Ag:TiO_2 samples as a function of the annealing temperatures

According to the results shown in Fig. 5 it is possible to observe that as the Ag concentration increases the clusters starts to appear for lower temperatures and the grain size is tendentiously higher.

The sample with χ_{Ag} = 0.16 revealed a grain size of about 18 nm at 600 ºC, remaining very close to 20 nm for higher annealing temperatures. As the Ag content increases (χ_{Ag} = 0.24) the grain size is somewhat higher, increasing from about 24 nm (600 ºC) to 42 nm (800 ºC). Nevertheless, in both samples, no crystalline domains of Ag where detected for annealing temperature up to 500 ºC, as already discussed above.

In the case of χ_{Ag} = 0.35 the clusters start to crystallize at lower temperature. The grain size increases from about 18 nm (at 400 ºC) to almost 70 nm (at 800 ºC). Finally, the film with higher Ag content, χ_{Ag} = 0.40, revealed Ag clusters with about 22 nm already at 200 º C, remaining approximately constant up to 500 ºC. Then, it sharply increases up to 75 nm when the temperature rises to 800 ºC.

3.1.5 Influence of heat-treatment on the morphology of the films

According to the XRD analysis, one can divide the samples into two different groups (or zones) due to similarities found on their structural evolution with annealing temperature; a zone I which includes the samples with molar factions ranging from χ_{Ag} = 0.16 to 0.24, and a zone II, for the samples with molar factions between χ_{Ag} = 0.35 and 0.40. The morphological evolution of two sets of representative Ag:TiO_2 films, one of zone I and another ascribed to zone II, was investigated by SEM. The micrographs are displayed in Fig. 6 and show two major morphological modifications with the annealing temperature. The first is directly related with the Ag content dispersed in the TiO_2 host matrix, while the second might be correlated with the structural and morphological rearrangements that occurred as a result of the heat-treatment.

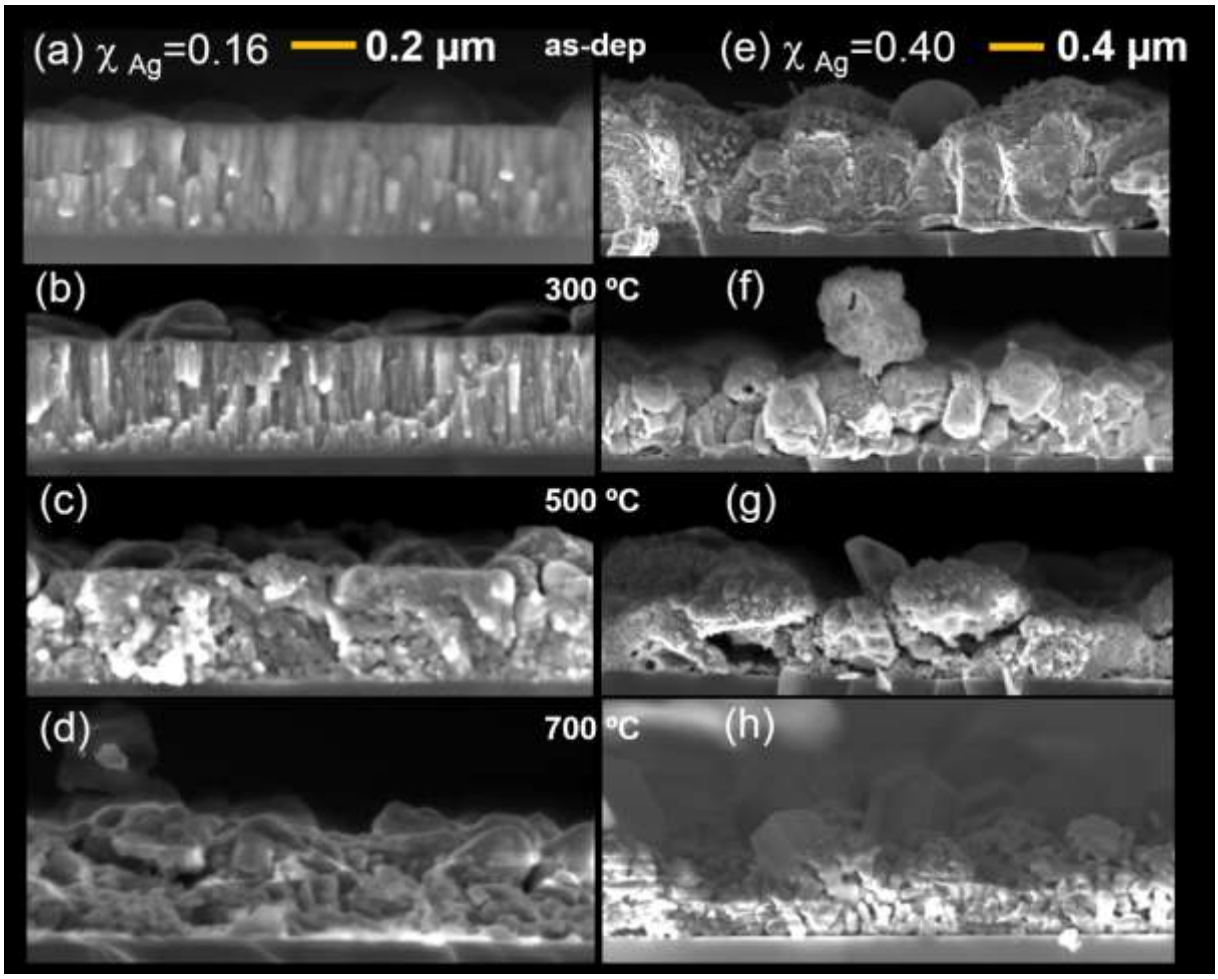

Figure 6 – Microstructural evolution with annealing temperature for different Ag molar fractions, (a-d) $\chi_{Ag} = 0.16$ and (e-h) $\chi_{Ag} = 0.40$.

As already observed in the SEM images depicted in Fig. 1, one could clearly observe that the typical columnar microstructure of the pure sputtered TiO_2 film changed to more disordered microstructures, becoming less compact and relatively more porous with the addition of Ag (see also the examples of Fig 6(a) and (e)). In particular, the highly disordered morphology observed for the samples with higher Ag content, such as the one displayed in Fig. 6(e) with $\chi_{Ag} = 0.40$, is a consequence of the enhancement of Ag atoms reaching the film during the early stages of its growth, creating favourable conditions for the formation of Ag clusters, as suggested by the SEM analysis. Furthermore, when the as-deposited samples are subjected to the annealing process there is a speed up of the diffusion processes, which leads to an increased size of the Ag clusters, inducing heterogeneous structures.

In the case of low Ag molar fraction ($\chi_{Ag} = 0.16$) the columnar growth is visible up to 300 ºC, nevertheless this microstructure seems to disappear for higher temperatures, and the coatings develop a more granular / voided microstructure. The formation of highly disordered

microstructures is even more clear in the sample with χ_{Ag} = 0.40, where the granular / voided morphology is already visible for the as-deposited sample. The heat-treatment promotes the aggregation of Ag clusters into larger crystalline domains throughout the matrix as well as in the outermost regions, as also claimed by other authors [30].

Another important feature about the sample with χ_{Ag} = 0.40 annealed at 700ºC (Fig. 6 (h)) is that the crystallization of rutile TiO_2 seemed to have promote the Ag diffusion along their grain boundaries, towards the surface of the film. The formation of large silver crystallites on the surface of the film was observed in more detail by SEM, as showed in Fig. 7. Some of the SEM images were acquired using the energy selective backscattered electron mode, showing that these grains have higher density than the surrounding matrix (Fig. 7(d) and (e)). The shape analysis of the Ag crystals performed by SEM suggests the formation of cuboctahedrons (faceted polyhedrons composed by triangular and square faces [32] [33]), with estimated average sizes of 1.1 μm (calculated by Feret analysis using ImageJ software). This type of structures have great potential in plasmonic applications such as in optical biosensing and surface enhanced Raman spectrometry (SERS), since the shape of the clusters plays also an important role on the properties of LSPR absorption band.

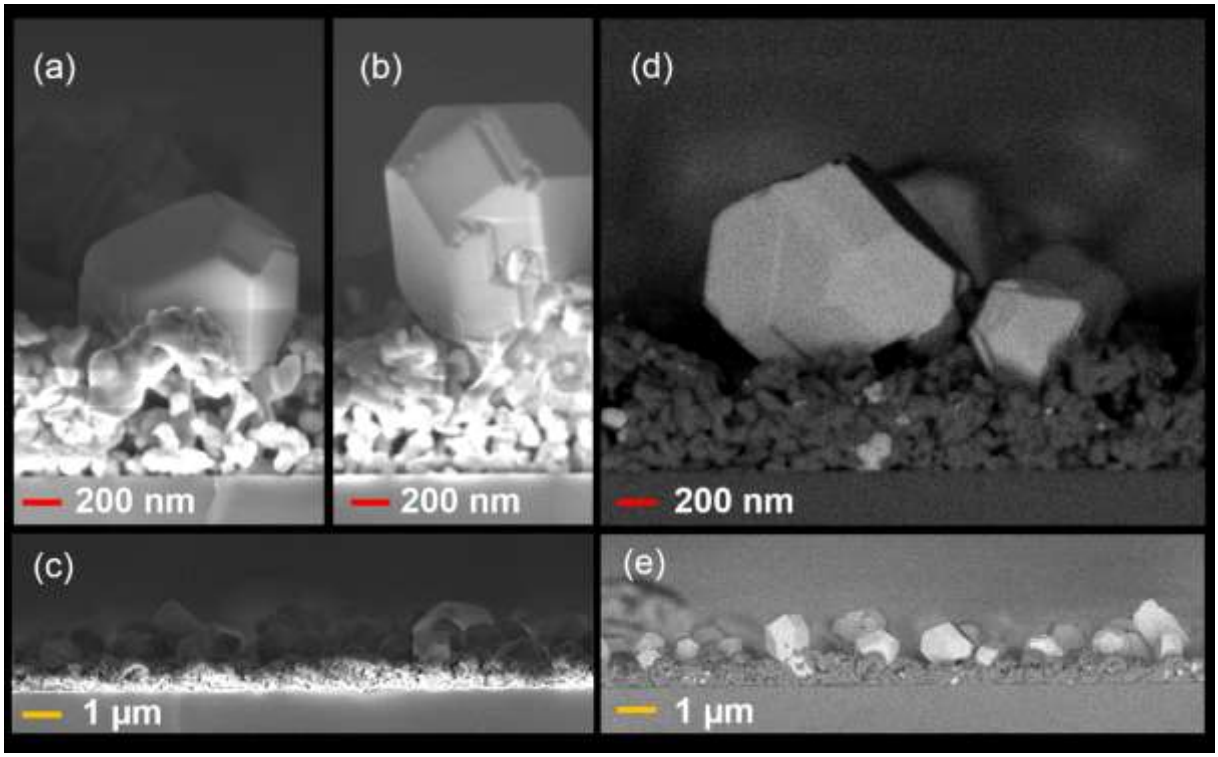

Figure 7 –cross section SEM using (a-c) in-lens secondary electron and (d-e) energy selective backscattered electron to have compositional contrast to confirm the higher density of the Ag grains. The size of the large Ag grains (cuboctahedrons) was estimated in 1.1.

Some features related with the microstructural evolution of the films are summarized in Fig. 8. The grain size of the crystalline domains of Ag is illustrated by the colour map embedded in the figure and the range of temperatures where the anatase and rutile TiO_2 phases were detected are also presented.

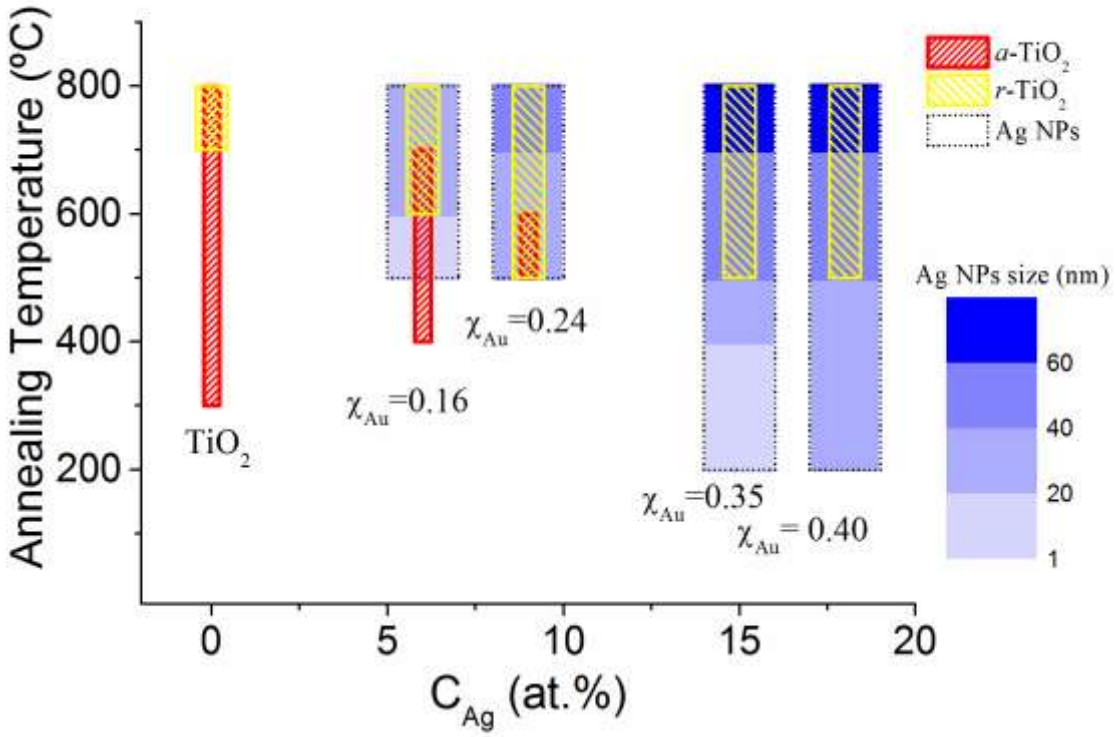

Figure 8 Diagram resuming the major microstructural characteristics of the Ag:TiO_2 films. It can be observed the range of annealing temperatures where the Ag clusters were detected for the different series of samples analysed; the evolution of the size of the crystalline domains of Ag as a function of the temperature for different compositions; and the range of temperatures where the anatase (*a*- TiO_2) and/or rutile (*r*- TiO_2) structures are present.

3.2 Optical properties of the Ag:TiO_2 films

In this section the main results of the optical behaviour are presented, namely the transmittance spectra of the different sets of films. The transmittance profiles are plotted in Fig. 9(a-d), only for selected temperatures where the major differences were observed.

Figure 9(a) shows the transmittance spectra of the sample with Ag molar fraction of χ_{Ag} = 0.16 (zone I). It is possible to observe an interference-like behaviour for the samples annealed up to 500 ºC influenced by the oxide matrix and due to the relatively low Ag content. For higher temperatures (between 600 and 800 ºC) the transmittance is lower and no interference fringes can be observed. The films become almost opaque, which can be a consequence of the silver segregation. Therefore, for low Ag content and under the conditions used no LSPR band could be reported. These results are in agreement with the XRD analysis, which did not show crystalline domains of Ag up to 500 ºC. Nevertheless, the XRD results also showed the formation of Ag clusters for higher temperatures, but probably they are not well distributed and separated in order to support localised surface plasmon resonances. When the molar fraction of Ag increases to χ_{Ag} = 0.24 (still in zone I), Fig. 8(b), the optical behaviour follows an identical trend as the previous sample, which was an expected behaviour since the structural and morphological evolution was also found to be very similar.

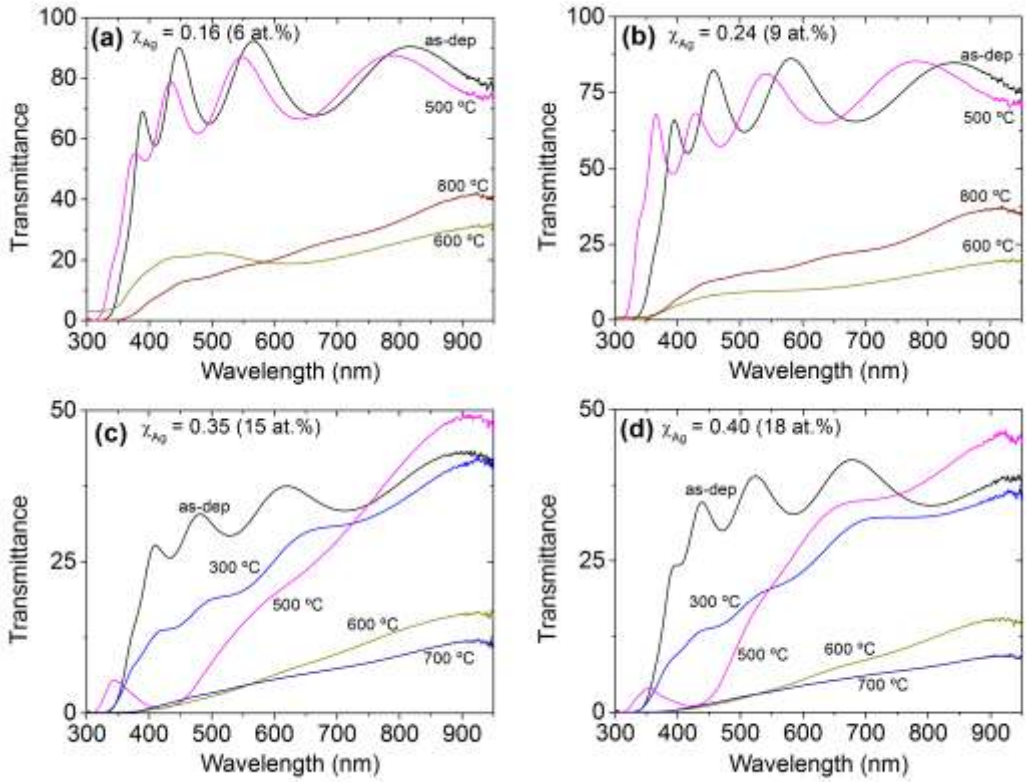

Figure 9 Transmittance spectra of the representative samples with a) χ_{Ag} = 0.16, b) χ_{Ag} = 0.24, c) χ_{Ag} = 0.35 and d) χ_{Ag} = 0.40, for a set of representative temperatures

As discussed in the previous sections, further increasing the Ag content induces major structural and morphological changes in the films, especially when they are subjected to heat-treatment. Figs. 9(c) and (d) show the transmittance spectra of the samples with Ag molar fraction of χ_{Ag} = 0.35 and χ_{Ag} = 0.40, respectively (both indexed to zone II), which follow similar trends in terms of optical behaviour, as expected, taking into account the microstructural analysis. In both cases it is possible to observe an interference-like behaviour for the samples annealed up to 300 ºC. Furthermore, for annealing temperature of 500 ºC the transmittance profile clearly shows a transmittance minimum at about ~420 nm, most probably due to LSPR absorption. This is the most important result of the optical analysis, which shows that it is possible to obtain LSPR peaks with Ag clusters dispersed in a TiO_2 matrix. It can also be reported that it is possible to shift the LSPR peak to lower wavelengths and hence tune the LSPR peak by replacing the plasmonic metal in the film; namely Au, which was studied in a recent work [13], for Ag, in the present case. Once again, these results are particular important if the envisaged applications of Ag:TiO_2 are plasmonic sensing or SERS, where the spectral region for effective detection might be important.

For higher annealing temperatures (between 600 and 800 ºC), Ag clusters with dozens of nm were formed, as demonstrated in Fig. 7. Their distribution seems to be unsuitable to support surface plasmon resonances in the visible range, nevertheless a transmittance minimum can be observed in the UV region at about 370 nm, just before the absorption edge of TiO_2 due to interband transitions. In this particular case, further investigation needs to be performed in order to better understand the optical behaviour of these films.

3.3 Thermal properties of the Ag:TiO_2 films

In order to study the influence of the microstructural evolution on the thermal properties of the Ag:TiO_2 system, the films were analyzed by modulated infrared radiometry (MIRR). This technique allows the determination of the thermal parameters of layered systems such as thin films and coatings [22] [34] [35] [36] [37].

Figure 10 shows the results obtained for two sets of samples representative of zones I and II, with molar fractions of (a) χ_{Ag} = 0.24 and (b) χ_{Ag} = 0.35, respectively. The samples were deposited in (i) glass and (ii) fused silica substrates. Theoretical simulations based on

the two-layer model proposed by Fotsing el al. [22] are represented by solid lines. According to the mentioned model the thermal diffusion time (τ_s), and the thermal effusivity ratio (e_c/e_b) between the film (c) and the substrate (b), rely on the values of the normalized phase lag (Φ_n), and the corresponding modulation frequency (f) at the extremum of the Φ_n *vs.* $f^{1/2}$ curves. As it can be observed, the theoretical curves fits very well the behavior obtained experimentally.

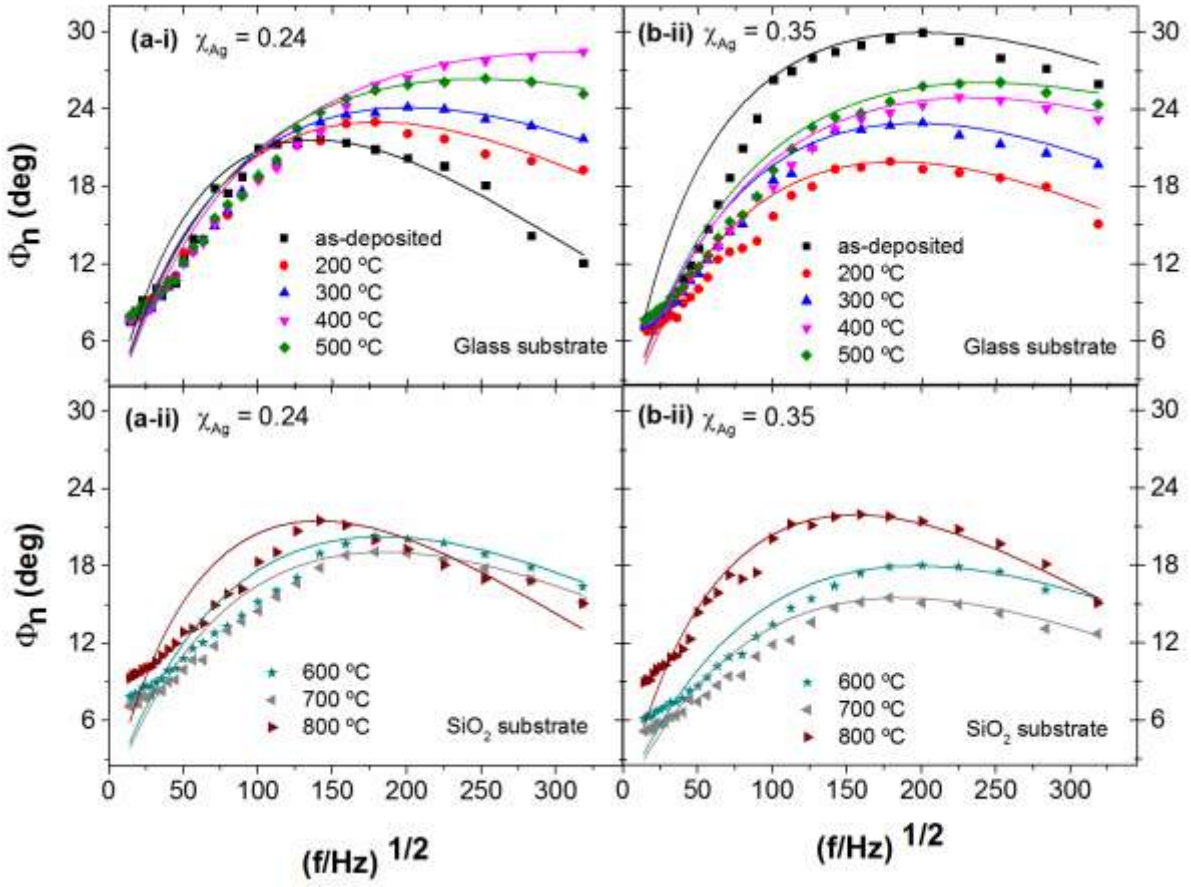

Figure 10. Inverse normalized phase lag *vs.* modulation frequency for two sets of Ag:TiO_2 films. The solid lines show simulations according to the two-layer model. The samples are deposited on (i) glass substrates – annealing temperatures up to 500˚C; and (ii) on fused silica substrates – annealing temperatures from 600 to 800˚C.

The thermal parameters obtained from the fits are presented in Table 1. From the analysis of those parameters, one can conclude that the thermal diffusivity of the films indexed to zone I (χ_{Ag} = 0.24) stays on relatively low values. As a general tendency, the thermal diffusivity and the effusivity ratios increase as the annealing temperature increases, for the films annealed up to 500 ºC, being much lower and decreasing very smoothly as the

annealing temperature further increases (between 600 ºC and 800 ºC). This decrease might be related with the silver diffusion to the surface, decreasing the thermal diffusivity of the thin film as a whole. Although there is a coincidence between the two trends observed for the thermal diffusivity and the replacement of the substrate where the samples were deposited (glass to fused silica), the changes observed cannot be directly attributed to this feature. In fact, the microstructural characterization of the films was performed in Si substrates up to 800 ºC and it was clearly demonstrated that for temperatures in the range 600-800 ºC there are major structural and morphological changes occurring, which can explain the differences observed in the thermal behavior.

The set of samples indexed to zone II (χ_{Ag} = 0.35) present similar trends in terms of thermal behavior when compared to those of zone I. In this case, the increase in the thermal diffusivity with the annealing temperature is even more pronounced for films deposited on glass. The values obtained for the thermal diffusivity are slightly higher when compared to the previous ones, reflecting the higher content of Ag. For the highest range of annealing temperatures (600-800 ºC) the calculated values, once again, drop more abruptly, due to the same effects already described for the samples with χ_{Ag} = 0.24; which are related to the diffusion and aggregation of Ag on the surface of the film

Table 1. Thermal parameters determined by MIRR, from the data in Fig. 10. Thermal diffusivity ($\alpha = d^2 / \tau$) values were calculated assuming the thickness estimated by SEM ($d_{(\chi Ag = 0.24)}$ = 0.50 μm; $d_{(\chi Ag = 0.35)}$ = 0.64 μm).

Substrate	**Annealing temperature (ºC)**	**Zone I (χ_{Ag} = 0.24)**			**Zone II (χ_{Ag} = 0.35)**		
		τ_s/μ_s	e_c/e_b	α_s / **10^{-7} (m^2/s)**	τ_s/μ_s	e_c/e_b	α_s / **10^{-7} (m^2/s)**
Glass	as dep	2.1	3.66	1.2	0.7	7.57	5.4
	200	1.2	4.05	2.1	1.2	3.24	3.3
	300	0.9	4.43	2.7	1.0	4.03	4.1
	400	-	-	-	0.7	4.73	6.1
Fused Silica	500	0.6	5.34	4.4	0.6	5.22	6.8
	600	1.2	3.32	2.1	1.1	2.83	3.7
	700	1.2	3.06	2.0	1.3	2.41	3.2
	800	2.0	3.63	1.3	1.6	3.74	2.5

The identified two trends for the thermal behaviour are clearly emphasized in Fig. 11, where the thermal diffusivity is plotted as a function of the annealing temperature.

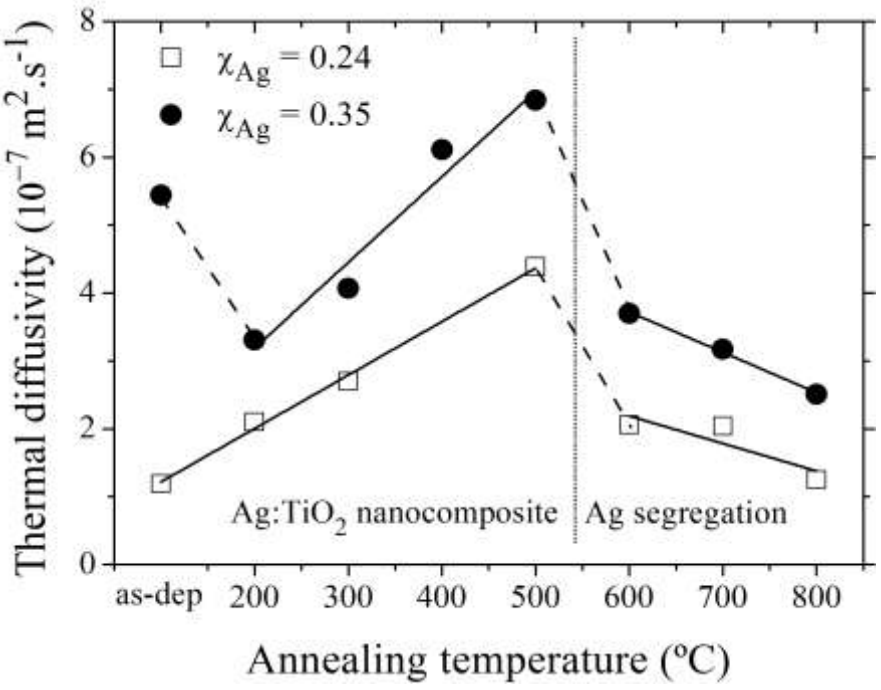

Figure 11. Thermal diffusivity *vs* annealing temperature for both χ_{Ag} = 0.24 and χ_{Ag} = 0.35 Ag:TiO_2 films.

In both sets of samples analyzed by MIRR, the simulations adjust better to the experimental data for the higher frequency ranges (Fig. 10). Due to the penetration depth dependence on the modulation frequency, the lower the modulation frequency used the higher will be the substrate contribution to the measured signal. As the modulation frequency increases, the contribution of the thin film to the measured signal becomes more important, therefore the theoretical curve will adjust better to the experimental data; while for lower frequencies, the influence of the substrate will become dominant. The fact that the substrate had to be changed for temperatures of 600 ºC and above, introduces an additional source of complexity when analyzing the experimental results. However, the changes observed are most likely due to the silver segregation, in agreement with the microstructural and optical properties results.

The higher values for the thermal diffusivity occur for the annealing temperature of 500 ºC, which was also the value where LSPR peaks were detected. This is certainly related with the transition from an amorphous phase to a polycrystalline structure, where the Ag

particles are homogeneously distributed throughout the matrix, reflecting a higher internal order and consequently a better diffusivity. The thermal effusivity ratio behaviour can be explained basically in the same way of what was explained for the thermal diffusivity.

The results obtained in this section can be understood as a contribution to a general characterization of the Ag:TiO_2 system. From that perspective, the major concern was to understand the trend of the thermal parameters rather than the precise determination of the thermal properties. It is worth to note that the results obtained for both sets of samples (χ_{Ag} = 0.24 and χ_{Ag} = 0.35) are coherent concerning the general evolution of the thermal properties, showing the reliability of the measurements performed, as well as the role of silver in the evolution of the thermal characteristics of the samples. The results obtained are also consistent with previous ones concerning the Au:TiO_2 system [35] [36], showing again the ability of MIRR to resolve thin films and coatings near the micrometer range.

Conclusions

In order to study the influence of silver concentration and annealing temperature on the microstructural evolution and physical responses of Ag:TiO_2 films, different sets of samples were prepared. Thin films with different Ag concentration were deposited using DC magnetron sputtering using a Ti target with small pellets of silver placed on the preferred erosion zone, and then subjected to a thermal (annealing) treatment in air atmosphere.

The discharge voltage (-V) of the Ti target was nearly independent of the number of Ag pellets placed in its preferential erosion zone, with values around 480-490 V. However, the increase of Ag pellets strongly influenced the growth rate of the films, especially for higher number of Ag pellets. While up to 3 pellets the growth rate remained approximately constant, close to 4 $nm.min^{-1}$, since the incorporation of Ag in the film was low, for higher number of pellets (up to 6) the growth rate sharply increased to about 10 $nm.min^{-1}$, due to morphological changes. In fact, the columnar growth of the films was gradually suppressed with the increase of Ag concentration giving rise to the formation of granular / voided structures. These morphological changes explain the differences observed in the growth rate evolution. As aimed, the atomic concentration of Ag incorporated in the film increased with the number of Ag pellets placed in the Ti target, varying between 6 at.% (χ_{Ag} = 0.16) and 18 at.% (χ_{Ag} = 0.40).

The annealing treatment strongly influenced the structural and morphological characteristics of the films, and hence affected their physical properties. Furthermore, the addition of Ag to the growing film delays the crystallization of anatase and lowers the transition temperature of rutile formation from amorphous/anatase TiO_2.

The segregation of Ag was very pronounced for annealing temperatures in the range 600-800 ºC, which affected the optical and thermal responses. For lower annealing temperatures ($\leq$ 500 ºC) the overall set of results seems to indicate the formation of a nanocomposite material, where Ag clusters/nanoparticles are embedded in the TiO_2 matrix. The appearance of LSPR peaks was clearly observed, but only for the highest Ag molar fractions (χ_{Ag} = 0.35 and 0.40) and for a short range of annealing temperatures (400-500 ºC).

A major conclusion that can be drawn from this work is that, under certain conditions, it is possible to obtain Ag:TiO_2 nanocomposite films with plasmonic properties. On the one hand, LSPR absorption bands can be obtained for low wavelengths (about 420 nm) and, on the other hand, unusual shapes for Ag crystals could also be reported (namely the Ag

cuboctahedrons), which might have great potential in plasmonic applications such as in optical biosensing and SERS.

Acknowledgements

This research was sponsored by FEDER funds through the COMPETE program (Programa Operacional Factores de Competitividade) and by FCT (Fundação para a Ciência e a Tecnologia), under the projects PEST-C/FIS/UI607/2013 and PEst-C/EME/UI0285/2013. The authors also acknowledge the financial support by the project Nano4color – Design and develop a new generation of color PVD coatings for decorative applications (FP7 EC R4SME Project No. 315286). J. Borges also acknowledges the support by the European social fund within the framework of realizing the project "Support of inter-sectoral mobility and quality enhancement of research teams at Czech Technical University in Prague", CZ.1.07/2.3.00/30.0034. C. Lopes acknowledges FCT for the PhD grant SFRH/BD/103373/2014. F.M. Couto acknowledges CAPES – Foundation, Ministry of Educaton of Brazil, Brasília – DF 70040-20, Brazil, funding by stage sandwich doctorate, through PDSE – Doctoral Program Sandwich.

References

[1] J. Toudert, L. Simonot, S. Camelio, D. Babonneau, Advanced optical effective medium modeling for a single layer of polydisperse ellipsoidal nanoparticles embedded in a homogeneous dielectric medium: Surface plasmon resonances, Physical Review B, 86 (2012) 045415.
[2] E. Petryayeva, U.J. Krull, Localized surface plasmon resonance: Nanostructures, bioassays and biosensing—A review, Analytica Chimica Acta, 706 (2011) 8-24.
[3] E. Hutter, J.H. Fendler, Exploitation of Localized Surface Plasmon Resonance, Advanced Materials, 16 (2004) 1685-1706.
[4] K.A. Willets, R.P. Van Duyne, Localized surface plasmon resonance spectroscopy and sensing, in: Annual Review of Physical Chemistry, Annual Reviews, Palo Alto, 2007, pp. 267-297.
[5] M.I. Stockman, Nanoplasmonics: The physics behind the applications, Phys. Today, 64 (2011) 39-44.
[6] R. Gradess, R. Abargues, A. Habbou, J. Canet-Ferrer, E. Pedrueza, A. Russell, J.L. Valdes, J.P. Martinez-Pastor, Localized surface plasmon resonance sensor based on Ag-PVA nanocomposite thin films, J. Mater. Chem., 19 (2009) 9233-9240.
[7] J. Homola, Surface plasmon resonance sensors for detection of chemical and biological species, Chem. Rev., 108 (2008) 462-493.
[8] M. Fan, G.F.S. Andrade, A.G. Brolo, A review on the fabrication of substrates for surface enhanced Raman spectroscopy and their applications in analytical chemistry, Analytica Chimica Acta, 693 (2011) 7-25.
[9] N.R. Agarwal, M. Tommasini, E. Fazio, F. Neri, R.C. Ponterio, S. Trusso, P.M. Ossi, SERS activity of silver and gold nanostructured thin films deposited by pulsed laser ablation, Appl. Phys. A, 117 (2014) 347-351.
[10] A.J. Haes, C.L. Haynes, A.D. McFarland, G.C. Schatz, R.R. Van Duyne, S.L. Zou, Plasmonic materials for surface-enhanced sensing and spectroscopy, MRS Bull., 30 (2005) 368-375.
[11] P. Etchegoin, Quo vadis surface-enhanced Raman scattering?, Physical Chemistry Chemical Physics, 11 (2009) 7348-7349.
[12] M. Torrell, R. Kabir, L. Cunha, M.I. Vasilevskiy, F. Vaz, A. Cavaleiro, E. Alves, N.P. Barradas, Tuning of the surface plasmon resonance in TiO2/Au thin films grown by magnetron sputtering: The effect of thermal annealing, Journal of Applied Physics, 109 (2011).
[13] R.M.S. Pereira, J. Borges, P.A.S. Pereira, G.V. Smirnov, F. Vaz, A. Cavaleiro, M.I. Vasilevskiy, Optical response of fractal aggregates of polarizable particles, in: Proceedings of SPIE - The International Society for Optical Engineering, 2014.
[14] J. Borges, T. Kubart, S. Kumar, K. Leifer, M.S. Rodrigues, N. Duarte, B. Martins, J.P. Dias, A. Cavaleiro, F. Vaz, Microstructural evolution of Au/TiO2 nanocomposite films: The influence of Au concentration and thermal annealing, Thin Solid Films, 580 (2015) 77-88.
[15] J. Borges, D. Costa, E. Antunes, C. Lopes, M.S. Rodrigues, M. Apreutesei, E. Alves, N.P. Barradas, P. Pedrosa, C. Moura, L. Cunha, T. Polcar, F. Vaz, P. Sampaio, Biological behaviour of thin films consisting of Au nanoparticles dispersed in a TiO2 dielectric matrix, Vacuum, (2015) In press.
[16] R.M.S. Pereira, J. Borges, P.A.S. Pereira, G.V. Smirnov, F. Vaz, A. Cavaleiro, M.I. Vasilevskiy, Optical response of fractal aggregates of polarizable particles, in, 2014, pp. 92865M-92865M-92868.
[17] R.M.S. Pereira, J. Borges, F.C.R. Peres, P.A.S. Pereira, G.V. Smirnov, F. Vaz, A. Cavaleiro, M.I. Vasilevskiy, Effect of clustering on the surface plasmon band in thin films of metallic nanoparticles, Journal of Nanophotonics, 9 (2015).
[18] J. Borges, N. Martin, N.P. Barradas, E. Alves, D. Eyidi, M.F. Beaufort, J.P. Riviere, F. Vaz, L. Marques, Electrical properties of AlNxOy thin films prepared by reactive magnetron sputtering, Thin Solid Films, 520 (2012) 6709-6717.
[19] N. Per-Erik, K. Svein Otto, Photothermal Radiometry, Physica Scripta, 20 (1979) 659.

[20] J. Gibkes, F. Vaz, A.C. Fernandes, P. Carvalho, F. Macedo, J. R. T. Faria, P. Kijamnajsuk, J. Pelzl, B.K. Bein, Analysis of multifunctional oxycarbide and oxynitride thin films by modulated IR radiometry, Journal of Physics D: Applied Physics, 43 (2010) 395301.
[21] F. Macedo, F. Vaz, L. Rebouta, P. Carvalho, A. Haj-Daoud, K.H. Junge, J. Pelzl, B.K. Bein, Modulated IR radiometry of (TiSi)N thin films, Vacuum, 82 (2008) 1457-1460.
[22] J.L. Nzodoum Fotsing, J. Gibkes, J. Pelzl, B.K. Bein, Extremum method: Inverse solution of the two-layer thermal wave problem, Journal of Applied Physics, 98 (2005) 063522.
[23] S. Mahieu, D. Depla, Reactive sputter deposition of TiN layers: modelling the growth by characterization of particle fluxes towards the substrate, Journal of Physics D: Applied Physics, 42 (2009) 053002.
[24] D. Depla, S. Heirwegh, S. Mahieu, J. Haemers, R. De Gryse, Understanding the discharge voltage behavior during reactive sputtering of oxides, Journal of Applied Physics, 101 (2007) 013301.
[25] D. Depla, S. Mahieu, R. De Gryse, Magnetron sputter deposition: Linking discharge voltage with target properties, Thin Solid Films, 517 (2009) 2825-2839.
[26] P. Pedrosa, D. Machado, C. Lopes, E. Alves, N.P. Barradas, N. Martin, F. Macedo, C. Fonseca, F. Vaz, Nanocomposite Ag:TiN thin films for dry biopotential electrodes, Applied Surface Science, 285, Part A (2013) 40-48.
[27] C. Lopes, P. Fonseca, T. Matamá, A. Gomes, C. Louro, S. Paiva, F. Vaz, Protective Ag:TiO2 thin films for pressure sensors in orthopedic prosthesis: The importance of composition, structural and morphological features on the biological response of the coatings, Journal of Materials Science: Materials in Medicine, 25 (2014) 2069-2081.
[28] V.S. Smentkowski, Trends in sputtering, Progress in Surface Science, 64 (2000) 1-58.
[29] M. Torrell, L. Cunha, A. Cavaleiro, E. Alves, N.P. Barradas, F. Vaz, Functional and optical properties of Au:TiO2 nanocomposite films: The influence of thermal annealing, Applied Surface Science, 256 (2010) 6536-6542.
[30] R.C. Adochite, D. Munteanu, M. Torrell, L. Cunha, E. Alves, N.P. Barradas, A. Cavaleiro, J.P. Riviere, E. Le Bourhis, D. Eyidi, F. Vaz, The influence of annealing treatments on the properties of Ag:TiO2 nanocomposite films prepared by magnetron sputtering, Applied Surface Science, 258 (2012) 4028-4034.
[31] A.A. Mosquera, J.L. Endrino, J.M. Albella, XANES observations of the inhibition and promotion of anatase and rutile phases in silver containing films, Journal of Analytical Atomic Spectrometry, 29 (2014) 736-742.
[32] X. Xia, J. Zeng, L.K. Oetjen, Q. Li, Y. Xia, Quantitative Analysis of the Role Played by Poly(vinylpyrrolidone) in Seed-Mediated Growth of Ag Nanocrystals, Journal of the American Chemical Society, 134 (2012) 1793-1801.
[33] J. Zeng, Y. Zheng, M. Rycenga, J. Tao, Z.-Y. Li, Q. Zhang, Y. Zhu, Y. Xia, Controlling the Shapes of Silver Nanocrystals with Different Capping Agents, Journal of the American Chemical Society, 132 (2010) 8552-8553.
[34] M. Apreutesei, C. Lopes, J. Borges, F. Vaz, F. Macedo, Modulated IR radiometry for determining thermal properties and basic characteristics of titanium thin films, Journal of Vacuum Science and Technology A: Vacuum, Surfaces and Films, 32 (2014).
[35] F. Macedo, F. Vaz, M. Torrell, J. R. T. Faria, A. Cavaleiro, N.P. Barradas, E. Alves, K.H. Junge, B.K. Bein, TiO_2 coatings with Au nanoparticles analysed by photothermal IR radiometry, Journal of Physics D: Applied Physics, 45 (2012) 105301.
[36] F. Vaz, F. Macedo, R.T. Faria, Jr., M. Torrell, A. Cavaleiro, K.H. Junge, B.K. Bein, Modulated IR Radiometry Applied to Study TiO_2 Coatings with Gold Nanocluster Inclusions, Int J Thermophys, 34 (2013) 1597-1605.
[37] C. Lopes, C. Gonçalves, J. Borges, T. Polcar, M.S. Rodrigues, N.P. Barradas, E. Alves, E. Le Bourhis, F.M. Couto, F. Macedo, C. Fonseca, F. Vaz, Evolution of the functional properties of titanium-silver thin films for biomedical applications: Influence of in-vacuum annealing, Surface and Coatings Technology, 261 (2015) 262-271.